CANCER GENOMICS & PROTEOMICS *22*: 510-524 (2025)
doi: 10.21873/cgp.20518

C1orf50 Drives Malignant Melanoma Progression Through the Regulation of Stemness

YUSUKE OTANI[1,2*], MASAKI MAEKAWA[1,2*], ATSUSHI TANAKA[1,2*], TIRSO PEÑA[1,2], VANESSA D. CHIN[3], ANNA ROGACHEVSKAYA[1,2], SHINICHI TOYOOKA[4], MICHAEL H. ROEHRL[1,2] and ATSUSHI FUJIMURA[5,6]

[1]Department of Pathology, Beth Israel Deaconess Medical Center, Boston, MA, U.S.A.;
[2]Harvard Medical School, Boston, MA, U.S.A.;
[3]UMass Chan Medical School, UMass Memorial Medical Center, Worcester, MA, U.S.A.;
[4]Department of General Thoracic Surgery and Breast and Endocrinological Surgery, Okayama University Graduate School of Medicine, Dentistry and Pharmaceutical Sciences, Okayama, Japan;
[5]Department of Molecular Physiology, Kagawa University Faculty of Medicine, Graduate School of Medicine, Kagawa, Japan;
[6]Department of Cellular Physiology, Okayama University Graduate School of Medicine, Dentistry and Pharmaceutical Sciences, Okayama, Japan

Abstract

Background/Aim: Recent advancements in omics analysis have significantly enhanced our understanding of the molecular pathology of malignant melanoma, leading to the development of novel therapeutic strategies that target specific vulnerabilities within the disease. Despite these improvements, the factors contributing to the poor prognosis of patients with malignant melanoma remain incompletely understood. The aim of this study was to investigate the role of *C1orf50* (Chromosome 1 open reading frame 50), a gene previously of unknown function, as a prognostic biomarker in melanoma.
Materials and Methods: We performed comprehensive transcriptome data analysis and subsequent functional validation of the human Skin Cutaneous Melanoma project from The Cancer Genome Atlas (TCGA).
Results: Elevated expression levels of *C1orf50* correlated with worse survival outcomes. Mechanistically, we revealed that C1orf50 plays a significant role in the regulation of cell cycle processes and cancer cell stemness, providing a potential avenue for novel therapeutic interventions in melanoma.
Conclusion: This study is the first to identify *C1orf50* as a prognostic biomarker in melanoma. The clinical relevance of our results sheds light on the importance of further investigation into the biological mechanisms underpinning C1orf50's impact on melanoma progression and patient prognosis.

Keywords: C1orf50, melanoma, cancer stem cells, YAP/TAZ.

[*]These Authors equally contributed to this work.

Atsushi Fujimura, MD, Ph.D., Department of Molecular Physiology, Kagawa University Faculty of Medicine, Graduate School of Medicine, 1750-1 Ikenobe, Miki-cho, Kita-gun, Kagawa, 761-0793, Japan. Tel: +81 878912095, e-mail: fujimura.atsushi@kagawa-u.ac.jp

Received April 24, 2025 | Revised May 2, 2025 | Accepted May 5, 2025

Introduction

Recent advancements in cancer therapy have been achieved not only through traditional genetic analysis methods but also *via* the emergence of multi-omics approaches, significantly facilitating the discovery of novel therapeutic targets (1-5). Integrating multiple omics datasets have enabled detailed analyses of tumor molecular profiles at the individual patient level, thereby advancing personalized medicine (6). Despite these advancements, the incidence of malignant melanoma continues to rise. Even with the development of new molecularly targeted therapies and immunotherapies for primary skin tumors, melanoma remains a highly lethal disease (7, 8). To further improve the prognosis of patients with melanoma, it is crucial to identify novel therapeutic targets beyond current treatment options. In this context, we have focused on the previously uncharacterized gene *C1orf50*. Although *C1orf50* has been identified as a protein coding gene (9), and shown to be involved in breast cancer prognosis (10), specifically, biological roles and underlying mechanisms have remained mainly unknown. In the Human Protein Atlas (Version 23), high expression of *C1orf50* is considered prognostic, and is associated with an unfavorable prognosis in malignant melanoma. Our study utilized transcriptome data from The Cancer Genome Atlas (TCGA) melanoma project to investigate the potential association between *C1orf50* and the prognosis of melanoma patients. Our analysis suggests that *C1orf50* may regulate cancer cell stemness, a critical factor in tumor recurrence and treatment resistance. We hypothesize that *C1orf50* contributes to these processes by modulating cancer stem cell properties, thereby influencing the progression and prognosis of melanoma. To explore this hypothesis, we conducted a series of cellular experiments using malignant melanoma cell lines to elucidate the functions of *C1orf50*, specifically examining the effects of *C1orf50* knockdown on cancer stemness. Our findings indicate that *C1orf50* plays a role in maintaining cancer stem cell characteristics, which could contribute to the aggressive nature and poor prognosis of malignant melanoma. These analyses help to improve treatment outcomes by identifying new therapeutic targets and prognostic factors in malignant melanoma.

Materials and Methods

TCGA data acquisition. All analyses utilizing TCGA transcriptome data, including counts and transcripts per kilobase million (TPM) values, were conducted using R (version 4.3.2, University of Auckland, Auckland, North Island, New Zealand). Transcriptome and clinical data from TCGA Skin Cutaneous Melanoma (TCGA-SKCM) dataset were retrieved using the R package, TCGAbiolinks (version 2.30.0). Based on mRNA TPM values, primary melanoma samples were categorized into two groups – *C1orf50*-low (n=62) and *C1orf50*-high (n=41) – based on mRNA TPM values, with the cutoff point determined to achieve the minimum *p*-value in the log-rank test. The downstream analysis of transcriptome data employed log-transformed TPM values [Log2(TPM+1)]. One sample in the *C1orf50*-low group lacked survival data.

Differential expression analysis and gene set enrichment. Differential expression analysis was performed using transcriptome count data from the TCGA dataset, utilizing edgeR (version 4.0.7). Fold change values and q-values were calculated to determine significant differences between the specified groups. For the C1orf50 comparison, primary melanoma samples were divided into *C1orf50*-low (n=62) and *C1orf50*-high (n=41) groups. To identify enriched pathways and biological processes, clusterProfiler (version 4.10.1) was employed with ranked gene lists ordered by fold change values. Gene sets from the Molecular Signature Database (MSigDB, v2023.2.Hs) were used to perform enrichment tests and calculate normalized enrichment scores (NES) for each term. For functional characterization of each sample, we performed gene set variation analysis (GSVA) with MSigDB *via* the R GSVA package (version 1.50.1) and the calculated enrichment scores of gene sets for each sample.

Protein-protein interaction analysis. For the top 500 genes with the largest fold changes between the *C1orf50*-high and *C1orf50*-low groups, protein-protein interaction enrichment analysis was performed with the following databases: STRING6, BioGrid7, OmniPath8, InWeb_IM9. When the network contains more than three proteins, the Molecular Complex Detection (MCODE) algorithm was applied to identify densely connected network components.

Mutation data acquisition and mutation signature analysis. Mutation Annotation File (MAF) files were downloaded using TCGAbiolinks. Mutation frequencies between the *C1orf50*-high and *C1orf50*-low groups were compared using bar plots created with maftools (version 2.18.0). Mutational signatures and tumor mutation burden were calculated using COSMIC (v100).

Cell cultures and treatments. Human melanoma cell lines A2058, G-361, and Mewo were obtained from the Japanese Collection of Research Bioresources (JCRB, Ibaraki, Osaka, Japan) and cultured in Dulbecco's modified Eagle's medium (DMEM, Fujifilm-Wako, Osaka, Osaka, Japan) supplemented with 10% fetal bovine serum (FBS, Corning, Corning, NY, USA) and 1% penicillin/streptomycin/L-glutamine (Fujifilm-Wako).

RNAi experiments were performed using either siRNA or shRNA. For siRNA transfection, Lipofectamine RNAiMAX and Opti-MEM (Thermo Fisher Scientific, Waltham, MA, USA) were used. The following siRNA sequences were used in this study, listed as (Target gene/Source/Identifier): (negative control/Thermo Fisher Scientific/4390844); (human C1orf50/Thermo Fisher Scientific/s35534); (human C1orf50/Thermo Fisher Scientific/s35535); (human C1orf50/Thermo Fisher Scientific/s35536). For the preparation of lentiviruses harboring shRNA, 293FT cells were transfected with pLKO.1-puro backbone plasmid, psPAX2, and pMD2.G using TransIT-LT1 (TaKaRa Bio, Kusatsu, Shiga, Japan). The virus-containing medium was harvested and filtered with a polysulfone membrane. The following sequences of shRNA were used in this study: Control (CCTAAGGTTAAGTCGCCCTCG); Human C1orf50 #1 (CTGCACCATGTAGCTTGTAAT); Human C1orf50 #2 (GTCAGTCAGTTTCAGAGTATT).

Sphere-formation assay. The sphere-formation assay experiments were performed as previously reported with minor modifications. The cells were trypsinized and resuspended in serum-free medium, Neurobasal medium supplemented with 1×B-27 supplement, 1×N-2 supplement, 20 ng/ml human epidermal growth factor (Fujifilm-Wako), 20 ng/ml human basic fibroblast growth factor (Fujifilm-Wako), 10 μg/ml heparin (Sigma-Aldrich, St. Louis, MO, USA) and 1% penicillin/streptomycin/L-glutamine). A total of 1,000 cells per well were seeded on ultra-low attachment 24-well plates (Corning) in 1.5 ml of serum-free medium and cultured for seven days at 37˚ in an atmosphere of 5% CO_2.

Immunofluorescent analysis and confocal microscopy. Immunofluorescent analysis of melanoma cells was performed as previously described (11) with minor modifications. Briefly, cells fixed with 4% paraformaldehyde (PFA) for 15 min at room temperature (approximately 25˚) and blocked with 1% bovine serum albumin in phosphate-buffered saline (BSA-PBS) for 1 h at room temperature. Then, the samples were incubated with the primary antibody diluted with BSA-PBS for 16 h at 4˚C. The samples were washed three times with PBS and incubated with the secondary antibodies diluted with BSA-PBS for 1 h. After three washes with PBS, the samples were embedded with DAPI Fluoromount-G (Southern Biotech Co., Ltd., Birmingham, AL, USA). Immunofluorescent analysis on the melanoma tissue array was performed as previously described (12). The melanoma tissue array was purchased from TissueArray.com (catalog number: ME1921, Derwood, MD, USA). After deparaffinization and antigen retrieval with HistoVT One (Nacalai Tesque, Kyoto, Japan), the slide was blocked and stained as described above. The stained samples were observed using a confocal microscope, LSM780 (Carl Zeiss AG, Neubeuern, Rosenheim, Germany) and analyzed with ZEN software (Carl Zeiss AG). The

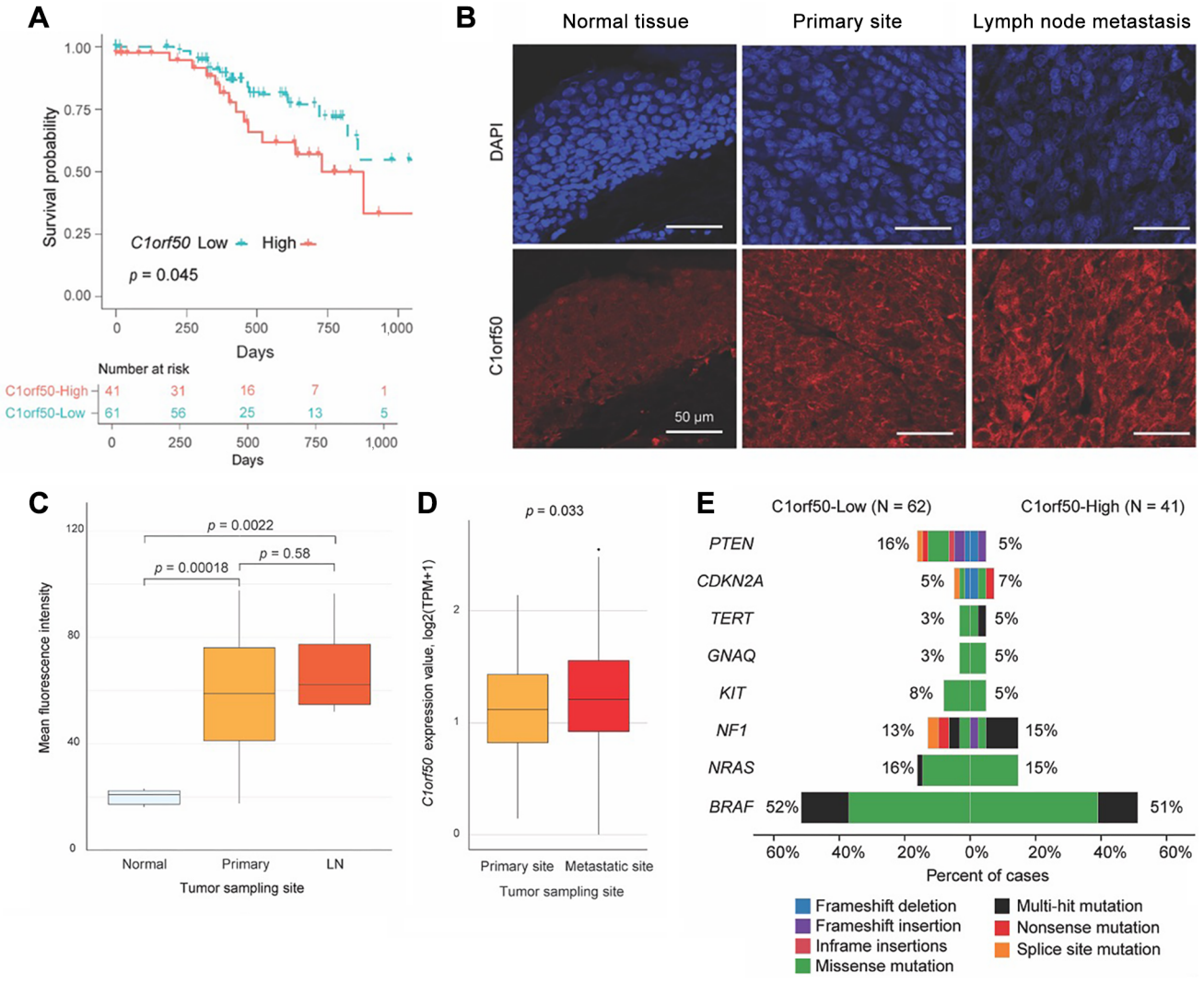

Figure 1. *Continued*

analyses of mean fluorescent intensity were performed with ImageJ software (National Institutes of Health, Bethesda, MD, USA). The following antibodies are used in immunofluorescent analyses, listed as (Antigen/Source/Identifier/Dilution): [C1orf50/Proteintech (Rosemont, IL, USA)/20957-1-AP/1:100]; [YAP-TAZ/Santa Cruz (Dallas, TX, USA)/sc-101199/1:50]; [TAZ/BD Biosciences (Franklin Lakes, NJ, USA)/560235/1:50]; (SOX-2/Santa Cruz/Y-17/1:100); (Donkey anti-mouse IgG Alexa Fluor Plus 488/Thermo Fisher Scientific/A32766/1:500); (Donkey anti-rabbit IgG Alexa Fluor Plus 594/Thermo Fisher Scientific/A32754/1:500); (Donkey anti-goat IgG Alexa Fluor Plus 647/Thermo Fisher Scientific/A32849/1:500).

Western blotting analysis. Western blotting experiments were performed as previously described (13). Protein extracts were obtained using cell lysis buffer [20 mM Tris-HCl (pH 7.5), 150 mM NaCl, 1 mM EDTA, 1 mM EGTA, 1% Triton X-100] and boiled in sample buffer [50 mM Tris-

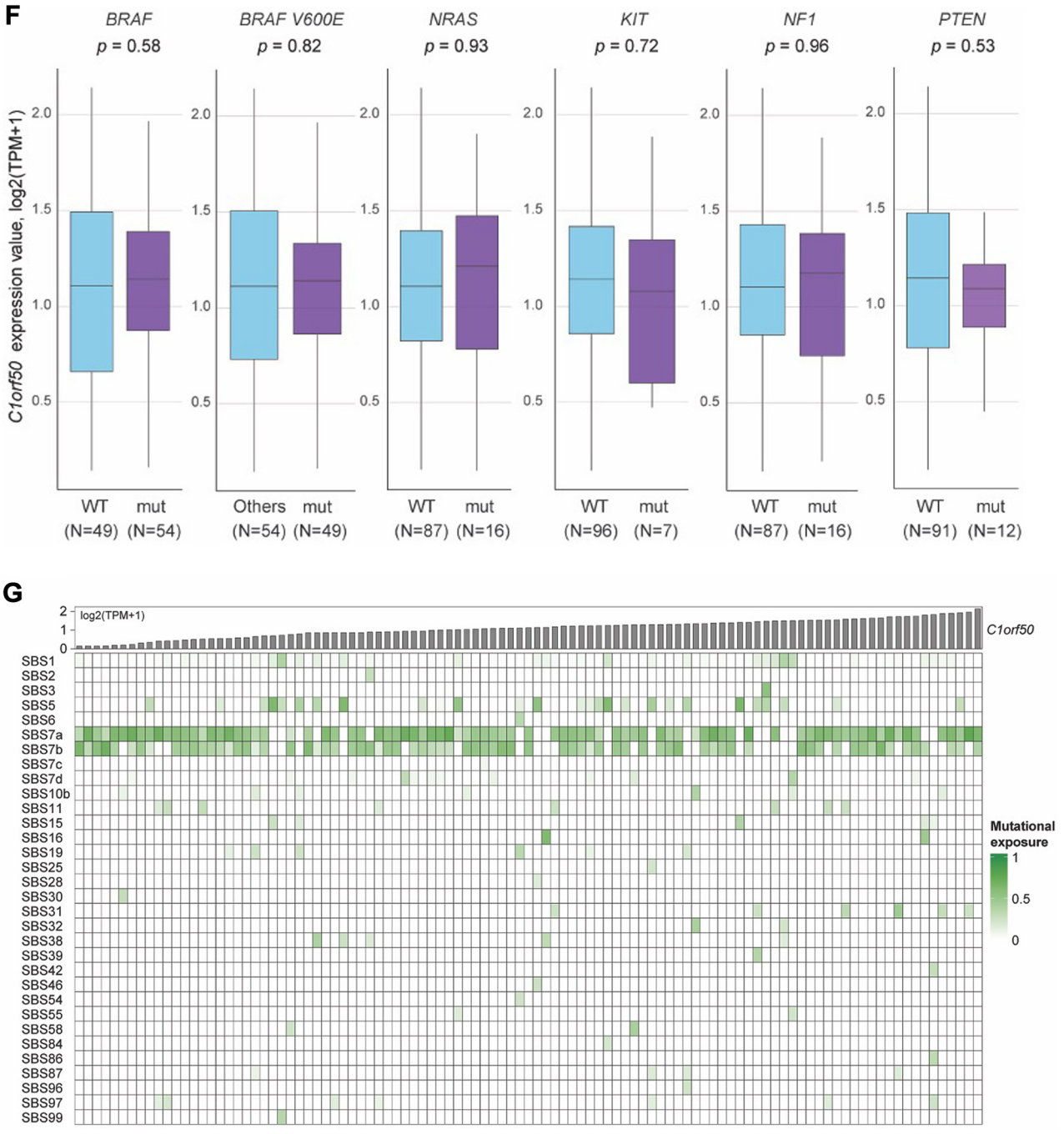

Figure 1. *Continued*

HCl (pH 6.5), 100 mM dithiothreitol, 2% SDS, 1.5 mM bromophenol blue, 1.075 M glycerol]. Equal amounts of proteins were loaded onto acrylamide gel and transferred onto Immobilon-P membrane (Millipore, Burlington, MA, USA). The membranes were blocked with 0.5% skim milk in Tris-buffered saline with tween20 (TBST) at room

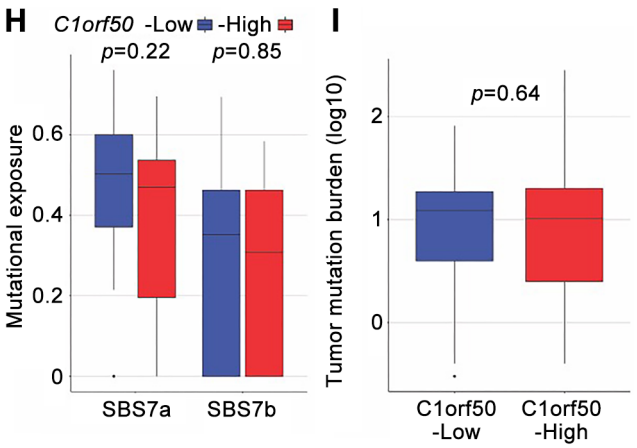

Figure 1. *Analysis of C1orf50 expression and its correlation with clinical and genomic features in primary malignant melanoma. (A) Kaplan–Meier curves for 3-year overall survival in the C1orf50-high and C1orf50-low groups of primary malignant melanoma. (B, C) Mean fluorescence intensity of C1orf50 in primary tumors and lymph node metastases compared to normal tissues. (D) Expression level of C1orf50 in metastatic sites (n=368) versus primary sites (n=103) in the TCGA Skin Cutaneous Melanoma (TCGA-SKCM) dataset. (E) Barplot showing mutation frequencies in the C1orf50-high and C1orf50-low groups. (F) Boxplot depicting changes in C1orf50 values depending on mutations in BRAF, BRAF V600E, NRAS, KIT, NF1, and PTEN. WT: Wild Type, mut: mutation. (G) Heatmap illustrating expression levels of single-base substitutions in COSMIC. (H) Differences between C1orf50-low and C1orf50-high groups in SBS7a and7b. (I) Tumor mutation burden (log10) differences between C1orf50-high and C1orf50-low groups. COSMIC: Catalogue Of Somatic Mutations In Cancer; SBS: single-base substitution.*

temperature for 1 h and incubated with the primary antibodies diluted with 0.1% skim milk in TBST for 16 h at 4˚. After three brief TBST washes, the membranes were incubated with HRP-conjugated secondary antibodies for 1 h at room temperature. The signals were developed with Clarity Western enhanced chemiluminescence substrate (Bio-Rad, Hercules, CA, USA) and were detected using a ChemiDoc Touch Imaging System (Bio-Rad). The following antibodies were used in this study, listed as (Antigen/Source/Identifier/Dilution): (C1orf50/Proteintech/20957-1-AP/1:100); (Vinculin/Proteintech/66305-1-Ig/1:20,000); (YAP-TAZ/Santa Cruz/sc-101199/1:2,000); (AXL/CST/4939/1:2,000); (CYR61/CST/39382/1:2,000); (c-MYC/CST/5605/1:2,000); (Nestin/Sigma-Aldrich/N5413-100UG/1:2,000); (SOX-2/Santa Cruz/Y-17/1:2,000); (CD133/Proteintech/18470-1-AP/1:2,000); (Anti-Mouse IgG, HRP-linked/Sigma-Aldrich/A9044/1:20,000); (Anti-Rabbit IgG, HRP-linked/CST/7074/1:2,000); (Anti-Goat IgG, HRP-linked/Sigma-Aldrich/A4174/1:20,000).

Statistical analysis. Comparisons of numerical values between two groups were performed using the Wilcoxon Test. Comparisons of numerical values between three or more groups were performed using one-way ANOVA (analysis of variance) with Bonferroni's multiple comparisons. The comparison test details are written in each figure legend. A *p*-value less than 0.05 was considered to be statistically significant. The significance levels are defined as **p*<0.05, ***p*<0.01, ****p*<0.001, NS.: not significant. The Kaplan-Meier curves were visualized using the survminer R package (version 0.4.9). The log-rank test was used to compare the two groups, *C1orf50*-high and *C1orf50*-low, in all survival analyses. The box plots were created using the ggpubr package (version 0.6.0) in R. In the heatmaps, we used Spearman's rank correlation coefficient to assess the strength and direction of association between two ranked variables.

Results

Impact of C1orf50 expression on the survival of patients with melanoma and tissue-specific expression analysis. Analysis of 102 primary malignant melanoma samples for whom survival data from TCGAbiolink was available showed that *C1orf50* expression levels significantly influenced patient survival. Patients were classified into groups based on high and low *C1orf50* expression. A comparison of 3-year survival rates showed a statistically significant difference, with *C1orf50*-high showing a worse prognosis (*p*=0.045) (Figure 1A). Further analysis of samples of patients with human melanoma showed that C1orf50 protein expression levels, measured by mean fluorescence intensity (MFI), were significantly higher in both primary and lymph node metastatic tissues than in normal tissues (Figure 1B and C). Furthermore, a comparison of *C1orf50* mRNA expression levels between 103 primary and 368 metastatic site samples from the TCGA dataset revealed that *C1orf50*

expression was significantly elevated in metastatic sites (p=0.033) (Figure 1D). These results suggest a potential association between *C1orf50* expression and prognosis in patients with melanoma.

Association of C1orf50 expression with genomic mutations. Considering the known association between gene mutations such as *BRAF*, *NRAS*, and *KIT* and tumor progression in melanoma (14), we examined whether mutation frequencies differed between the high and low *C1orf50* expression groups. Our analysis did not reveal significant differences in the overall mutation profile in the high *C1orf50* group compared to the low *C1orf50* group (Figure 1E). Using Fisher's exact test, we analyzed the frequency of mutations associated with melanoma progression and treatment; however, no statistically significant differences were found. Specifically, we observed no significant differences in *C1orf50* expression levels based on the presence or absence of all *BRAF* mutations, the *BRAF* V600E mutation alone, and mutations in *NRAS*, *KIT*, *NF1*, and *PTEN* (Figure 1F). We further analyzed mutational signatures in the *C1orf50* high and low groups using data from the Catalogue Of Somatic Mutations In Cancer (COSMIC) version 100. Analysis of COSMIC single-base substitution (SBS) signatures, including SBS7a and SBS7b – associated with sun-exposed skin cancers – showed no significant differences between the two groups (Figure 1G and H). Additionally, there was no significant difference in tumor mutation burden between the high and low *C1orf50* groups (Figure 1I). These data suggest that there is no association of *C1orf50* expression with well-known genetic mutations in melanoma biology.

Pathway analysis and protein-protein interaction (PPI) network analysis. To elucidate the molecular mechanisms by which C1orf50 promotes melanoma progression, we conducted pathway analysis using the TCGA melanoma dataset. The study divided patients with primary malignant melanoma into *C1orf50*-high and *C1orf50*-low groups, following the classifications used in the Kaplan-Meier survival analysis in the section Materials and Methods. Gene Set Enrichment Analysis (GSEA) revealed up-regulation of gene sets related to "Cell cycle" and "Melanoma" in the *C1orf50*-high group (Figure 2A). Additionally, gene sets associated with "Signaling pathways regulating pluripotency of stem cells" were highly expressed, suggesting a role of C1orf50 in stem cell pluripotency. The HALLMARK gene sets showed notable up-regulation in "G2M_CHECKPOINT", "MITOTIC_SPINDLE", and "E2F_TARGETS" in the *C1orf50*-high group (Figure 2B). These results imply a strong association between C1orf50 and the regulation of the cell cycle and maintenance of cancer stem cell properties. Using Metascape (v3.5.20240101), we performed protein-protein interaction enrichment analysis for further exploration. We selected the top 500 genes with the largest fold changes between the *C1orf50*-high and *C1orf50*-low groups for this analysis. This analysis identified protein modules related to embryonic morphogenesis, tissue morphogenesis, actin-mediated cell contraction, cell cycle, cell division, calcium signaling pathway, and ABC transporters (Figure 2C). These motifs are consistent with the expression patterns observed in the *C1orf50*-high group.

Impact of C1orf50 on cell cycle and DNA repair. Given the up-regulation of cell cycle-related pathways in the C1orf50-high group of primary melanoma (Figure 2), we further investigated the RNA expression levels of genes and pathways associated with the cell cycle (Figure 3A). Consistent with the predictions from pathway analysis, we observed a correlation between *C1orf50* RNA levels and cell cycle-related genes and pathways, as shown in the heatmap. Additionally, gene expression of *CDK1-9* except *CDK2*, *5*, *9* showed a significant increase in the *C1orf50*-high expression group (Figure 3B). Furthermore, in the heatmap (Figure 3A), the pathway score of GOBP_CELL_CYCLE calculated by Gene Set Variation Analysis (GSVA) positively correlated with *C1orf50* expression level (ρ=0.56, p<0.001). We also noted an elevation in the expression of DNA damage sensor genes (*ATM*, *ATR*) and downstream genes (*BRCA1*/*BRCA2*, *RAD50*, *RAD51*, *RAD52*, *etc*.) (Figure 3C). These findings suggest that cells with high *C1orf50* expression could

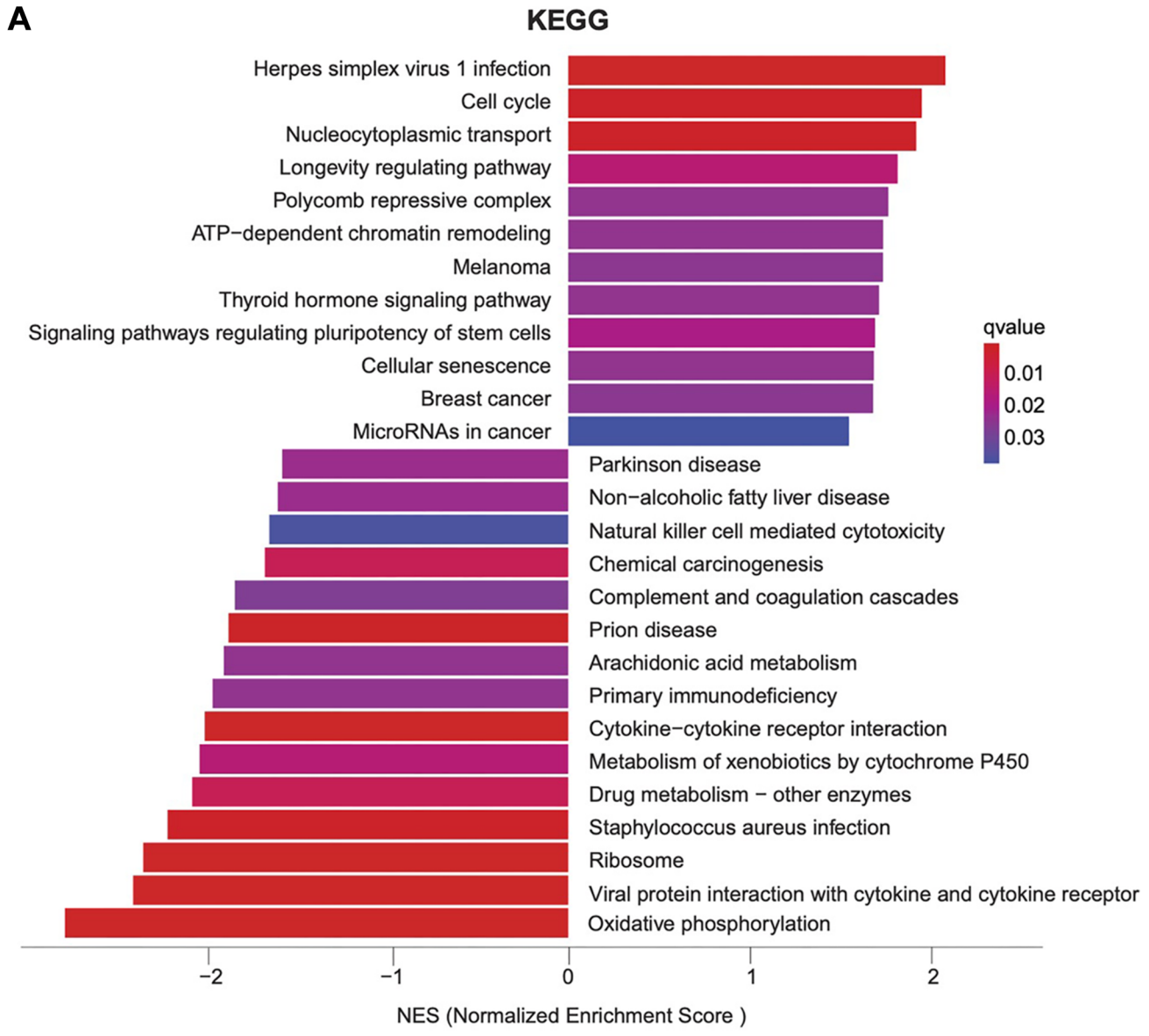

Figure 2. *Continued*

exhibit increased cell cycle activity and enhanced DNA damage repair mechanisms, as observed in primary malignant melanoma samples from the TCGA dataset.

Association of C1orf50 expression with cancer stemness and YAP-related pathways. The previously observed up-regulation of stemness-related terms in KEGG pathways (Figure 2A) and embryonic morphogenesis in PPI networks (Figure 2C) led us to investigate the potential role of C1orf50 in cancer stem cell traits. Additionally, since PPI analysis indicated the up-regulation of proteins related to actin-mediated cell contraction, we focused on YAP1/TAZ (yes-associated protein 1/transcriptional coactivator with PDZ-biding motif), a mechanotransducer regulated by actin

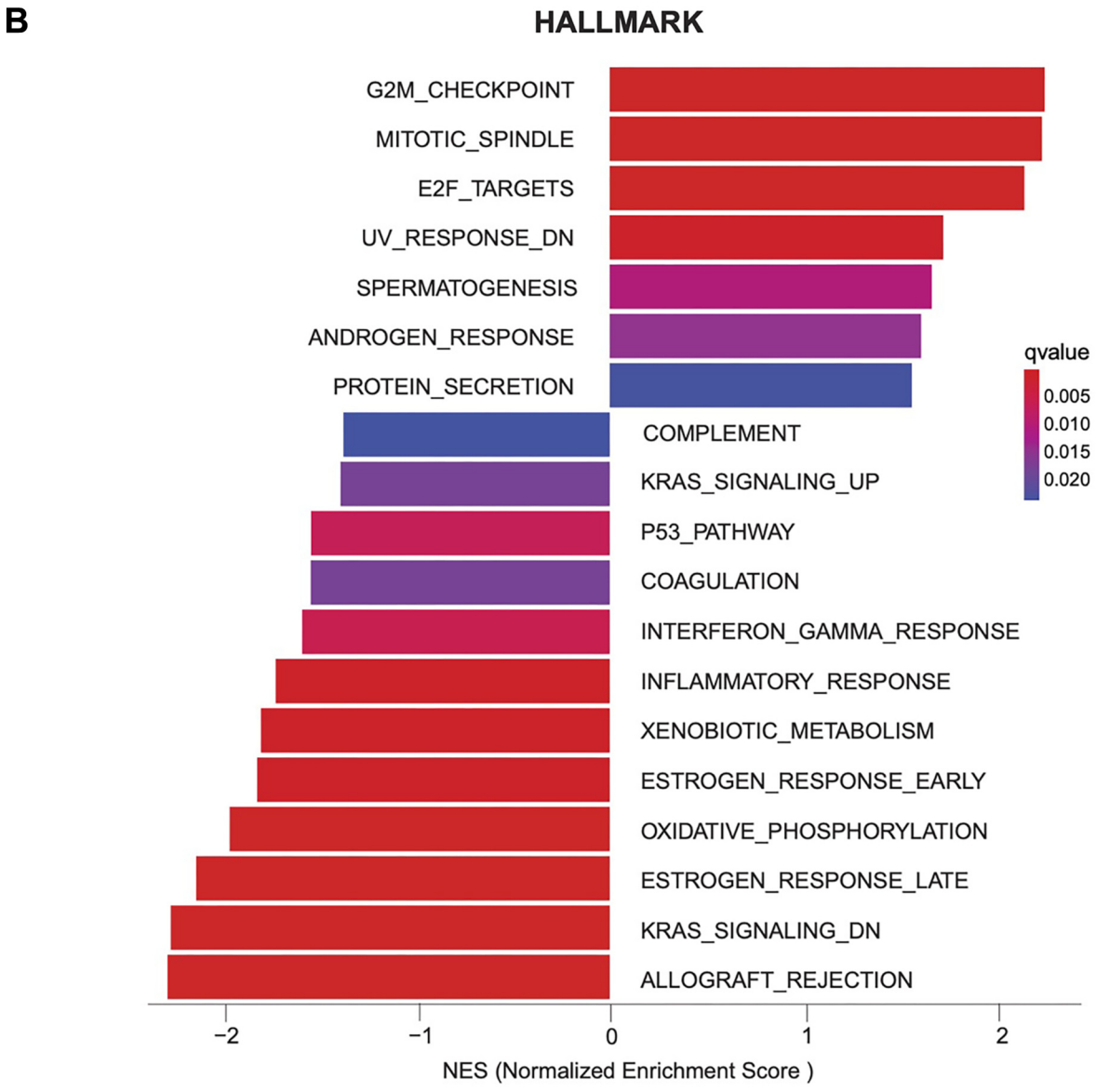

Figure 2. *Continued*

(15, 16). YAP1/TAZ interacts with the cytoskeleton, specifically actin, and is critical in regulating cell shape and movement. In melanoma, YAP1/TAZ is involved in the YAP1/PAX3/MITF and YAP1/TEAD/SMAD pathways (17). *C1orf50* expression correlated significantly with these genes and stem cell markers (Figure 3D). Furthermore, genes with a Spearman rank correlation coefficient of 0.2 or higher with *C1orf50* expression, excluding CCN2, showed significant expression differences in the YAP1/TEAD/SMAD and YAP1/PAX3/MITF pathways, as well as in cancer stem cell markers, based on Wilcoxon rank-sum test comparisons between the two groups (Figure 3E and F). These data indicate that *C1orf50* determines melanoma stem cell-related properties *via* YAP/TAZ activation.

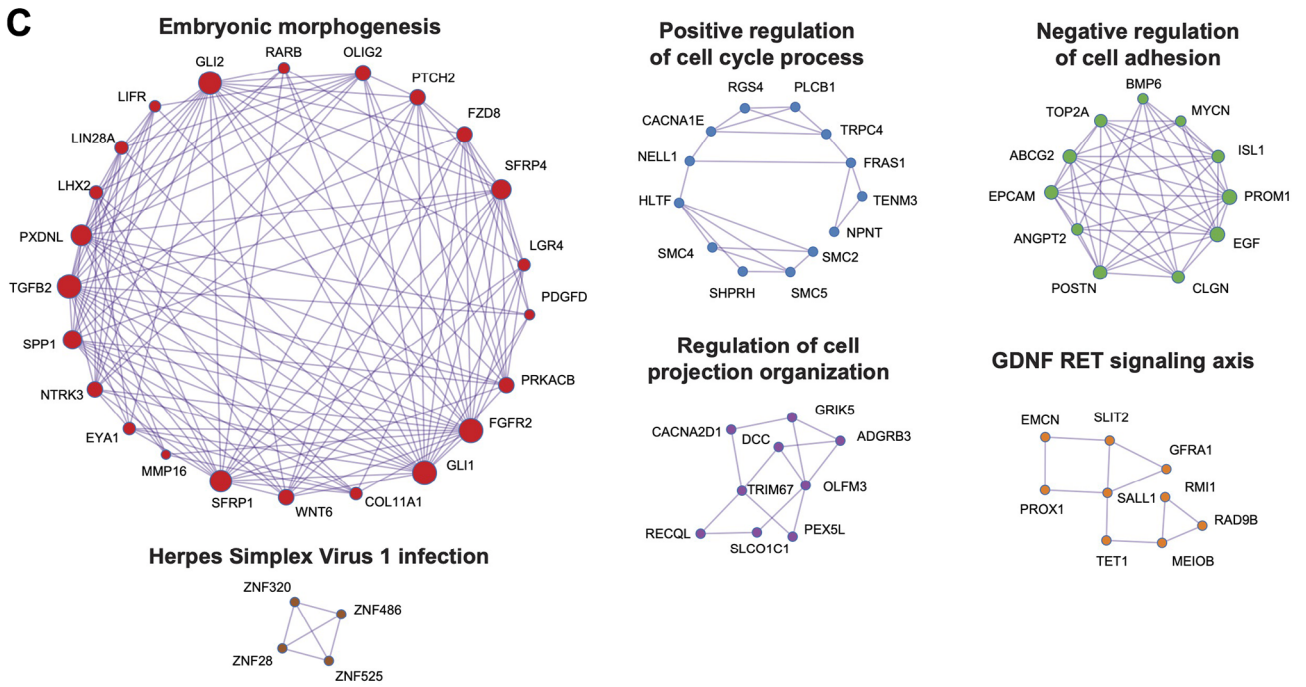

Figure 2. *Gene set enrichment analysis and protein-protein interaction analysis in the C1orf50-high group of primary malignant melanoma. (A) Gene Set Enrichment Analysis (GSEA) of Kyoto Encyclopedia of Genes and Genomes (KEGG) gene sets highlighting pathways enriched in the C1orf50-high group. (B) GSEA of HALLMARK gene sets showing pathways enriched in the C1orf50-high group. (C) Modules created from the top 500 genes with the highest fold change values in the C1orf50-high group compared to the C1orf50-low group, identified through Protein-Protein Interaction analysis.*

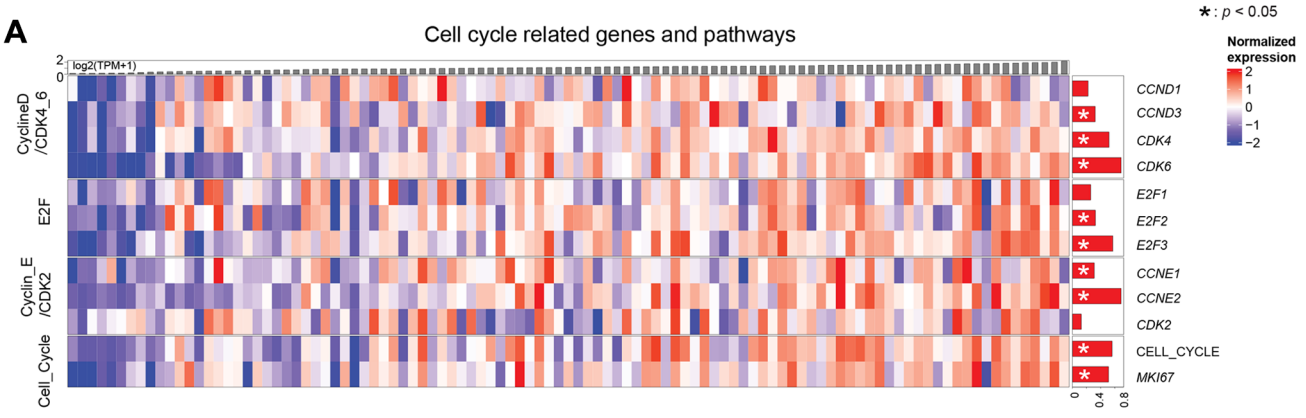

Figure 3. *Continued*

Functional validation of C1orf50 in melanoma stemness. To confirm the role of C1orf50 in maintaining melanoma stem cell-related traits, we used lentivirus expressing shRNA against *C1orf50* mRNA to infect melanoma the cell lines A2058, G-361, and Mewo. Protein extracts from infected cells were harvested three days post-infection, and immunoblotting was subsequently performed. *C1orf50* knockdown significantly reduced C1orf50 protein levels, indicating successful detection by the antibody used in this study (Figure 4A). The levels of YAP1, TAZ, and their target

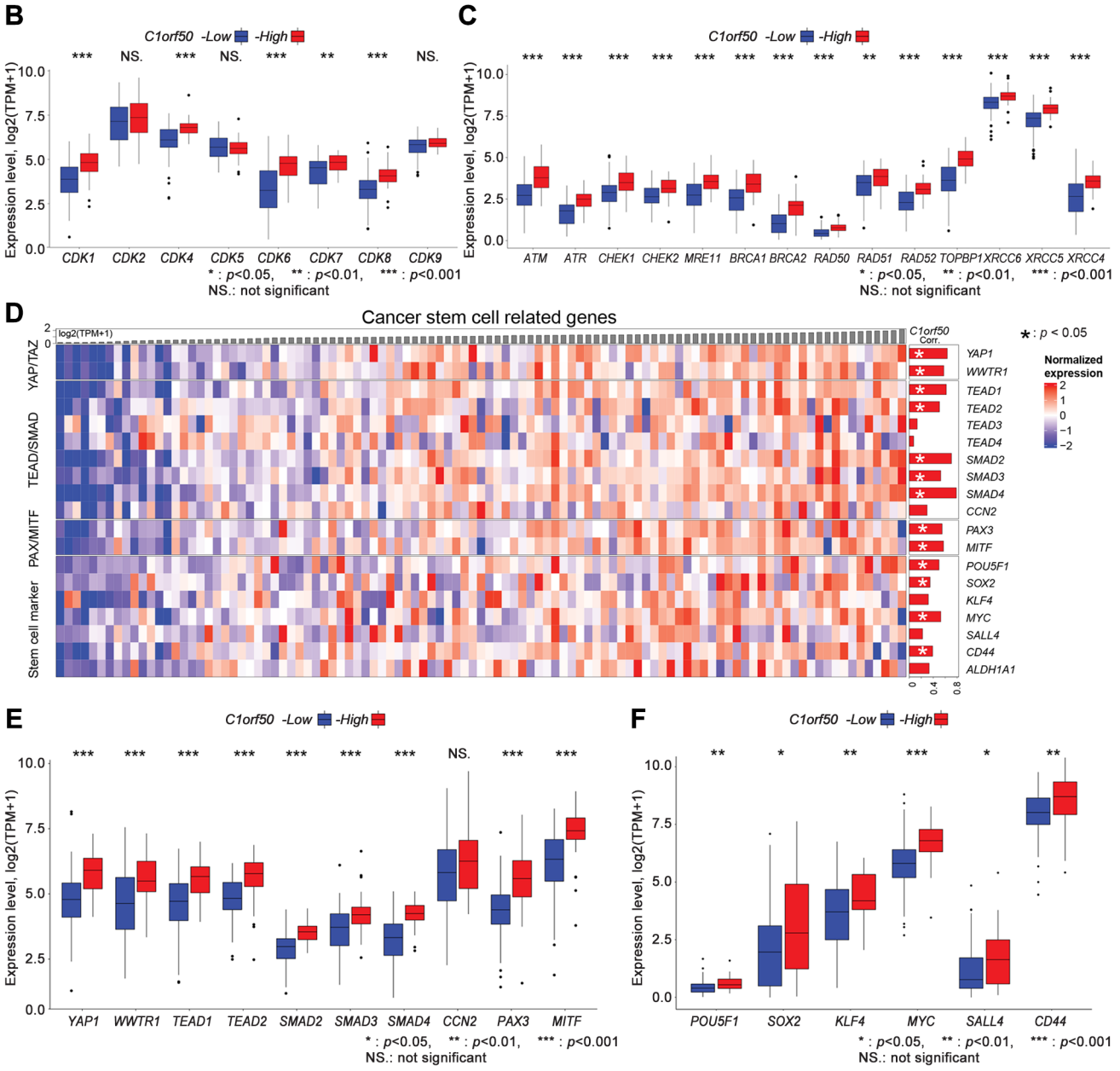

Figure 3. *Correlation of C1orf50 expression with cancer stem cell related genes and YAP/TAZ pathways. (A) Heatmap of cell cycle-related genes and pathways. (B) Comparison of detectable CDK1-9 genes between the C1orf50-high and C1orf50-low groups. (C) Comparison of DNA repair-related genes between the C1orf50-high and C1orf50-low groups. (D) Heatmap of cancer stem cell-related genes and pathways. (E) Comparison of YAP/TAZ-related genes between the C1orf50-high and C1orf50-low groups. (F) Comparison of cancer stem cell-related genes between the C1orf50-high and C1orf50-low groups.*

gene products AXL and CYR61 were decreased upon *C1orf50* knockdown (Figure 4A). Additionally, stemness markers CD133 (encoded by *PROM1*), NESTIN, SOX2, and c-MYC showed down-regulation. Sphere formation assays revealed that C1orf50 deficiency decreased self-renewal capacity in melanoma cells (Figure 4B). Given that

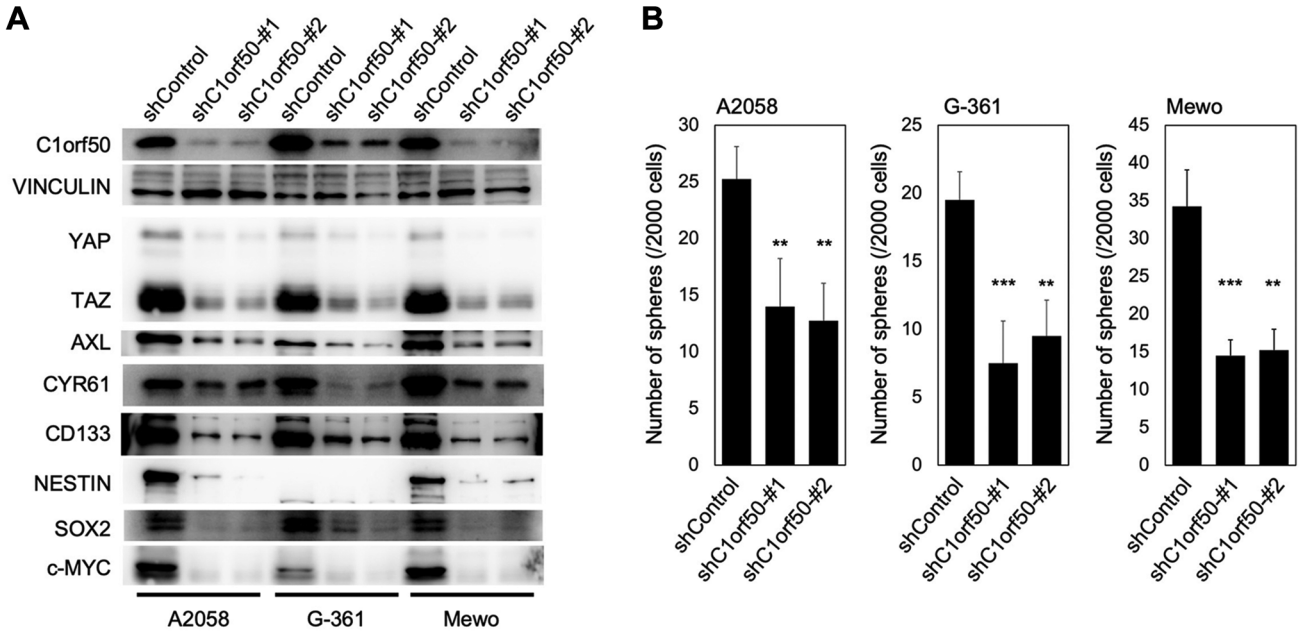

Figure 4. *Continued*

YAP1/TAZ activity is influenced by both protein amount and nuclear localization, loss of nuclear localization of YAP1/TAZ proteins in C1orf50-deficient A2058 and Mewo cells according to immunofluorescence analysis is compatible with sphere formation assay results (Figure 4C). Furthermore, to investigate the clinical relevance of C1orf50 expression in melanoma, we stained tissue arrays containing melanoma and normal skin tissues with anti-TAZ, C1orf50, and SOX2 antibodies. The mean fluorescence intensity (MFI) of C1orf50 correlated with TAZ and SOX2 in primary melanoma lesions (Figure 4D and E). These data indicate that the C1orf50 protein is required to maintain the YAP/TAZ activity and stemness in melanoma.

Discussion

In this study, we first demonstrated that *C1orf50* is a poor prognostic factor and that C1orf50 is higher at both mRNA and protein levels in primary melanoma tissues compared to normal tissues. We then confirmed that no correlation was found between *C1orf50* expression and commonly mutated genes in melanoma.

The pathway analysis revealed previously unknown associations of *C1orf50* expression with several essential pathways in malignant melanoma, including cell cycle regulation, DNA repair, and stem cell characteristics. Analysis of PPI also revealed characteristic motifs linked to embryonic and tissue morphogenesis, suggesting a connection between C1orf50 and cancer stem cell traits. Given the observed increase in actin-mediated cell contraction motifs, we focused on YAP1/TAZ, critical components in mechanotransduction (18). Further analysis in the TCGA malignant melanoma dataset indicated a potential link between C1orf50 and cancer stem cell characteristics, including markers like YAP1/TAZ. It is well-established that YAP1/TAZ activates TEAD transcription factors, which are critical in maintaining cancer stem cell properties (19-22). Additionally, in malignant melanoma, pathways involving YAP1 and PAX3 that regulate MITF are also significant. In the *C1orf50*-high group, an increase in YAP1/TAZ/TEAD and YAP1/PAX3/MITF pathways was observed. Through MITF, C1orf50 appears to play a role in processes such as anti-apoptosis, cell cycle regulation, and cell motility.

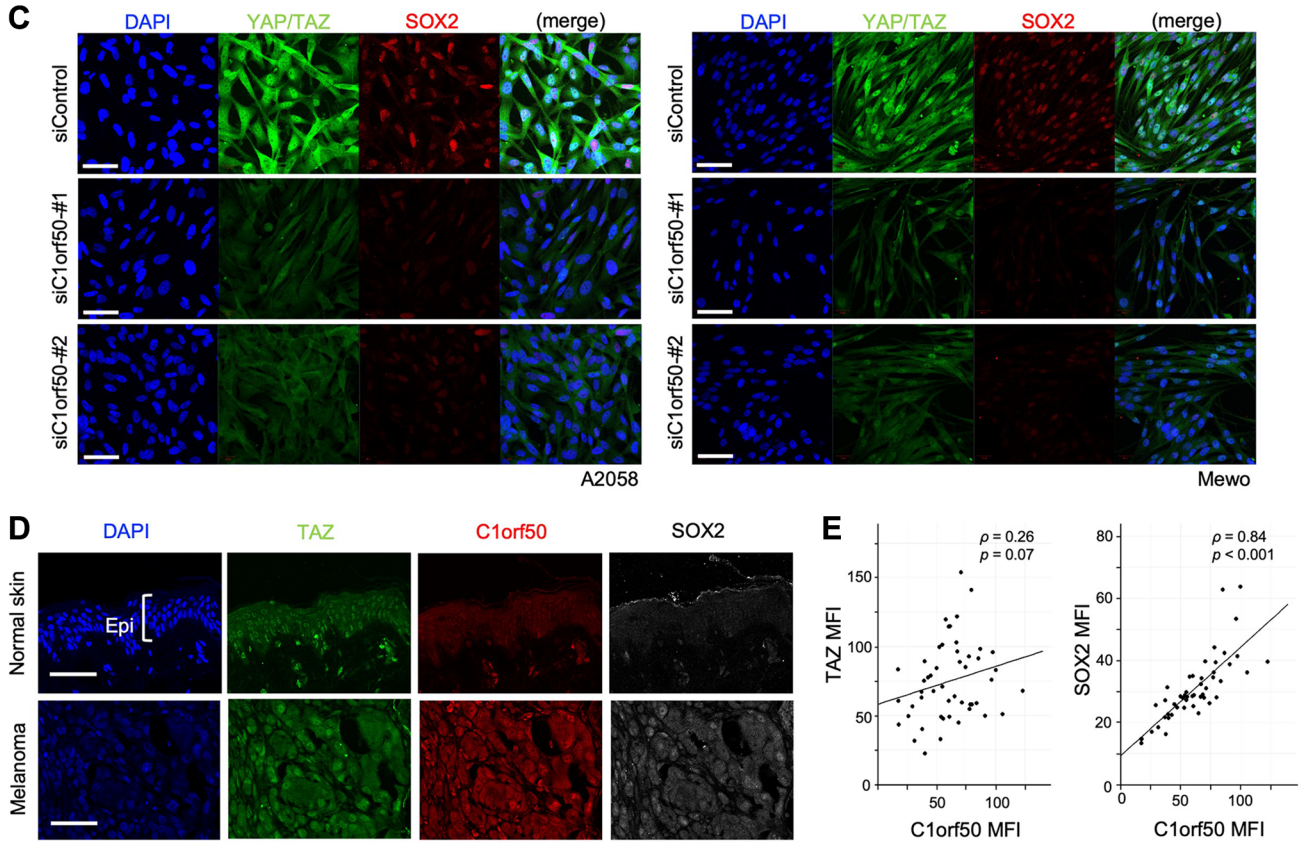

Figure 4. *Analysis of C1orf50 knockdown effects on stemness and YAP/TAZ pathways in malignant melanoma cells. (A) Representative images of immunoblotting analyses in shRNA-induced melanoma cells. C1orf50 knockdown reduces the expression levels of YAP/TAZ and their targets, AXL and CYR61, and the stemness markers CD133, NESTIN, SOX2, and c-MYC. Note that c-MYC signals were obtained after stripping and re-labeling the TAZ membrane. (B) Sphere formation assays in shRNA-transfected melanoma cells. C1orf50 is required to maintain the self-renewal capacity of melanoma cells. One-way ANOVA (analysis of variance) with Bonferroni's multiple comparisons was performed. The significance level was defined as **p<0.01, ***p<0.001. (C) Representative immunofluorescent images of siRNA-treated melanoma cells. C1orf50 knockdown attenuated the expression levels of YAP/TAZ and SOX2 in A2058 (left) and Mewo (right) cells. Note that the nuclear YAP/TAZ are merely observed in siC1orf50-treated cells, suggesting that C1orf50 maintains not only YAP/TAZ protein levels, but also YAP/TAZ activity: scale bars, 50 μm. The SOX2 immunostaining signals in Figure 4C were obtained with a combination of anti-SOX-2 goat antibody and anti-goat IgG Alexa Fluor Plus 647 and pseudo-colored with red using the ZEN software. (D) Representative immunofluorescent images of normal skin and melanoma tissues. The expression levels of C1orf50 are higher in the melanoma tissue than in the normal skin. In melanoma tissue, YAP/TAZ nuclear localization and SOX2 expression were enhanced. Scale bars, 50 μm. (E) Scatterplot graphs describing that the mean fluorescence intensity (MFI) of C1orf50 is correlated with that of TAZ (upper), or SOX2 (bottom) in melanoma primary lesions.*

To ensure that the observed associations were not merely due to co-expression with known prognostic factors, we knocked down *C1orf50* in melanoma cell lines and performed experiments. This approach clarified that C1orf50 regulates YAP/TAZ, contributing to stem cell traits in cancer. Previous studies by Nallet-Staub *et al*. have demonstrated that knockdown of YAP1/TAZ in melanoma cells results in a reduction of anchorage-independent growth, the capacity to invade Matrigel *in vitro,* and lung metastasis following tail vein injection of melanoma cells (23). Furthermore, YAP1 staining in human samples has been positively correlated with poor prognosis in patients with melanoma (24). Based on our analysis, C1orf50 is highly likely to regulate the stemness of melanoma through YAP1/TAZ, and controlling it could serve as a potential new therapeutic target for melanoma.

One limitation of this study is that the mechanisms by which C1orf50 is involved in cell cycle regulation and cancer stemness are unclear. Further experiments are needed to elucidate these pathways in greater detail. Our research highlights the potential clinical relevance of C1orf50 as a prognostic factor and a therapeutic target in melanoma, demonstrating its apparent impact on patient prognosis through clinical data.

Conclusion

This study identified *C1orf50* as a significant prognostic biomarker in malignant melanoma, linked to poor survival outcomes and cancer stem cell traits.

Conflicts of Interest

MHR is a member of Universal DX's Scientific Advisory Board. However, this company had no influence on support, design, execution, data analysis, or other aspects of this study.

Authors' Contributions

Yusuke Otani: Data curation; visualization; methodology; writing – original draft; writing – review and editing. Masaki Maekawa: Data curation; visualization; methodology; writing – original draft; writing – review and editing. Atsushi Tanaka: Data curation; visualization; methodology; writing – original draft; writing – review and editing. Tirso Peña: Data curation; writing – review and editing. Vanessa D. Chin: Data curation; writing – review and editing. Anna Rogachevskaya: Data curation; writing – review and editing. Shinichi Toyooka: Project administration; writing – review and editing. Michael H. Roehrl: Project administration; writing – review and editing. Atsushi Fujimura: Conceptualization; data curation; formal analysis; funding acquisition; investigation; methodology; project administration; resources; supervision; validation; writing – original draft; writing – review and editing.

Acknowledgements

The Authors are grateful to the Central Research Laboratory of Okayama University Medical School for their support with confocal microscopy. We thank all members of our laboratory for their valuable commitments to this study. The results published here are in whole, or part, based upon data generated by the TCGA Research Network.

Funding

This work was supported by a Grant-in-Aid for Scientific Research from the Ministry of Education, Culture, Sports, Sciences, and Technology of Japan (grant numbers: JP23K06676 to A.F.), the Japan Agency for Medical Research and Development (grant numbers: JP19cm0106143 and JP22cm0106179 to A.F.), and the Naito Foundation (A.F.).

Artificial Intelligence (AI) Disclosure

No artificial intelligence (AI) tools, including large language models or machine learning software, were used in the preparation, analysis, or presentation of this manuscript.

References

1 Benesch MGK, Cherkassky L, Nurkin SJ: Multi-omic analysis: a possible platform toward personalized and adaptable cancer treatment. Ann Surg Oncol 31(8): 4831-4833, 2024. DOI: 10.1245/s10434-024-15449-9

2 Krug K, Jaehnig EJ, Satpathy S, Blumenberg L, Karpova A, Anurag M, Miles G, Mertins P, Geffen Y, Tang LC, Heiman DI, Cao S, Maruvka YE, Lei JT, Huang C, Kothadia RB, Colaprico A, Birger C, Wang J, Dou Y, Wen B, Shi Z, Liao Y, Wiznerowicz M, Wyczalkowski MA, Chen XS, Kennedy JJ, Paulovich AG, Thiagarajan M, Kinsinger CR, Hiltke T, Boja ES, Mesri M, Robles AI, Rodriguez H, Westbrook TF, Ding L, Getz G, Clauser KR, Fenyö D, Ruggles KV, Zhang B, Mani DR, Carr SA, Ellis MJ, Gillette MA, Clinical Proteomic Tumor Analysis Consortium: Proteogenomic landscape of breast cancer tumorigenesis and targeted therapy. Cell 183(5): 1436-1456.e31, 2020. DOI: 10.1016/j.cell.2020.10.036

3 Tanaka A, Ogawa M, Zhou Y, Namba K, Hendrickson RC, Miele MM, Li Z, Klimstra DS, Buckley PG, Gulcher J, Wang JY, Roehrl MHA: Proteogenomic characterization of primary colorectal cancer and metastatic progression identifies proteome-based

subtypes and signatures. Cell Rep 43(2): 113810, 2024. DOI: 10.1016/j.celrep.2024.113810
4 Maekawa M, Tanaka A, Ogawa M, Roehrl MH: Propensity score matching as an effective strategy for biomarker cohort design and omics data analysis. PLoS One 19(5): e0302109, 2024. DOI: 10.1371/journal.pone.0302109
5 Tanaka A, Ogawa M, Zhou Y, Otani Y, Hendrickson RC, Miele MM, Li Z, Klimstra DS, Wang JY, Roehrl MH: Proteogenomic characterization of pancreatic neuroendocrine tumors uncovers hypoxia and immune signatures in clinically aggressive subtypes. iScience 27(8): 110544, 2024. DOI: 10.1016/j.isci.2024.110544
6 Du P, Fan R, Zhang N, Wu C, Zhang Y: Advances in integrated multi-omics analysis for drug-target identification. Biomolecules 14(6): 692, 2024. DOI: 10.3390/biom14060692
7 Robertson BM, Fane ME, Weeraratna AT, Rebecca VW: Determinants of resistance and response to melanoma therapy. Nat Cancer 5(7): 964-982, 2024. DOI: 10.1038/s43018-024-00794-1
8 Curti BD, Faries MB: Recent advances in the treatment of melanoma. N Engl J Med 384(23): 2229-2240, 2021. DOI: 10.1056/NEJMra2034861
9 MGC Project Team: The status, quality, and expansion of the NIH full-length cDNA project: the Mammalian Gene Collection (MGC). Genome Res 14(10B): 2121-2127, 2004. DOI: 10.1101/gr.2596504
10 Otani Y, Tanaka A, Maekawa M, Peña T, Rogachevskaya A, Ando T, Itano T, Katayama H, Nakata E, Ozaki T, Toyooka S, Doihara H, Roehrl MH, Fujimura A: The role of C1orf50 in breast cancer progression and prognosis. Breast Cancer 32(2): 292-305, 2025. DOI: 10.1007/s12282-024-01653-8
11 Fujimura A, Yasui S, Igawa K, Ueda A, Watanabe K, Hanafusa T, Ichikawa Y, Yoshihashi S, Tsuchida K, Kamiya A, Furuya S: In vitro studies to define the cell-surface and intracellular targets of polyarginine-conjugated sodium borocaptate as a potential delivery agent for boron neutron capture therapy. Cells 9(10): 2149, 2020. DOI: 10.3390/cells9102149
12 Huang R, Yamamoto T, Nakata E, Ozaki T, Kurozumi K, Wei F, Tomizawa K, Fujimura A: CDKAL1 drives the maintenance of cancer stem-like cells by assembling the eIF4F translation initiation complex. Adv Sci (Weinh) 10(12): e2206542, 2023. DOI: 10.1002/advs.202206542
13 Otani Y, Yoshikawa S, Nagao K, Tanaka T, Toyooka S, Fujimura A: Connective tissue mast cells store and release noradrenaline. J Physiol Sci 73(1): 24, 2023. DOI: 10.1186/s12576-023-00883-3
14 Kim HJ, Kim YH: Molecular frontiers in melanoma: pathogenesis, diagnosis, and therapeutic advances. Int J Mol Sci 25(5): 2984, 2024. DOI: 10.3390/ijms25052984
15 Dupont S, Morsut L, Aragona M, Enzo E, Giulitti S, Cordenonsi M, Zanconato F, Le Digabel J, Forcato M, Bicciato S, Elvassore N, Piccolo S: Role of YAP/TAZ in mechanotransduction. Nature 474(7350): 179-183, 2011. DOI: 10.1038/nature10137
16 Chang L, Azzolin L, Di Biagio D, Zanconato F, Battilana G, Lucon Xiccato R, Aragona M, Giulitti S, Panciera T, Gandin A, Sigismondo G, Krijgsveld J, Fassan M, Brusatin G, Cordenonsi M, Piccolo S: The SWI/SNF complex is a mechanoregulated inhibitor of YAP and TAZ. Nature 563(7730): 265-269, 2018. DOI: 10.1038/s41586-018-0658-1
17 Miskolczi Z, Smith MP, Rowling EJ, Ferguson J, Barriuso J, Wellbrock C: Collagen abundance controls melanoma phenotypes through lineage-specific microenvironment sensing. Oncogene 37(23): 3166-3182, 2018. DOI: 10.1038/s41388-018-0209-0
18 Piccolo S, Sladitschek-Martens HL, Cordenonsi M: Mechanosignaling in vertebrate development. Dev Biol 488: 54-67, 2022. DOI: 10.1016/j.ydbio.2022.05.005
19 Katayama H, Fujimura A, Huang R, Otani Y, Itano T, Fujiwara T, Kunisada T, Nakata E, Ozaki T: Role of catecholamine synthases in the maintenance of cancer stem-like cells in malignant peripheral nerve sheath tumors. Cancer Sci 115(3): 871-882, 2024. DOI: 10.1111/cas.16077
20 Battilana G, Zanconato F, Piccolo S: Mechanisms of YAP/TAZ transcriptional control. Cell Stress 5(11): 167-172, 2021. DOI: 10.15698/cst2021.11.258
21 Piccolo S, Panciera T, Contessotto P, Cordenonsi M: YAP/TAZ as master regulators in cancer: modulation, function and therapeutic approaches. Nat Cancer 4(1): 9-26, 2023. DOI: 10.1038/s43018-022-00473-z
22 Otani Y, Katayama H, Zhu Y, Huang R, Shigehira T, Shien K, Suzawa K, Yamamoto H, Shien T, Toyooka S, Fujimura A: Adrenergic microenvironment driven by cancer-associated Schwann cells contributes to chemoresistance in patients with lung cancer. Cancer Sci 115(7): 2333-2345, 2024. DOI: 10.1111/cas.16164
23 Nallet-Staub F, Marsaud V, Li L, Gilbert C, Dodier S, Bataille V, Sudol M, Herlyn M, Mauviel A: Pro-invasive activity of the Hippo pathway effectors YAP and TAZ in cutaneous melanoma. J Invest Dermatol 134(1): 123-132, 2014. DOI: 10.1038/jid.2013.319
24 Menzel M, Meckbach D, Weide B, Toussaint NC, Schilbach K, Noor S, Eigentler T, Ikenberg K, Busch C, Quintanilla-Martinez L, Kohlhofer U, Göke A, Göke F, Handgretinger R, Ottmann C, Bastian BC, Garbe C, Röcken M, Perner S, Kohlbacher O, Bauer J: In melanoma, Hippo signaling is affected by copy number alterations and YAP1 overexpression impairs patient survival. Pigment Cell Melanoma Res 27(4): 671-673, 2014. DOI: 10.1111/pcmr.12249